POLARIMETRIC-RAMAN LIDAR FOR TROPOSPHERIC ICE, LIQUID AND WATER VAPOR CONTENT. INSTRUMENT CONCEPT & DESIGN

G. Javier Fochesatto[1]*, Oscar Galvez[2], Rafael Escribano[2], Miguel A. Moreno[2] and Pablo Ristori[3]

*[1]Geophysical Institute, University of Alaska Fairbanks, AK 99775 USA,*Email: foch@gi.alaska.edu*

[2]Laboratorio de Fisica Molecular, Consejo Superior de Investigaciones Cientificas, Madrid, Spain

[3]Laboratorio Lidar. CITEDEF, Buenos Aires, Argentina.

ABSTRACT

We present the design of a new instrument that combines Raman spectroscopy and linear polarization analysis to identify the fraction of ice, liquid and water vapor in tropospheric aerosols and cloud layers. In this case water and ice fractions are obtained using the Raman N_2 line as reference. The instrument also measures the polarimetric S and P state of the backscattering lidar signal.

In this article an overview of the scientific applications of this instrument is given followed by a theoretical estimation of the lidar returns as well as the instrumental concept and design. First light of lidar profiles will be provided during conference.

1. INTRODUCTION

The thermodynamic state of water in the troposphere is influential and determining factor of major aerosol-cloud microphysical and dynamical processes. Spectrally resolved information of water in terms of amount of ice, liquid and vapor can be achieved by Laser spectroscopy (i.e., spontaneous Raman scattering). Such an instrument would be able to provide key information on specific cloud and aerosol processes but also to account for changes in the surrounding environment as cloud and aerosol layers evolve. Measuring the Raman shift up to ~3800 cm^{-1} with spectral resolution better than 1 cm^{-1} allows selection of discrete Raman bands and spectral lines to deduce the fractions of ice, liquid and water vapor over N_2 concentration present in the troposphere. Quantitative determination of concentration profiles requires knowing the Raman scattering cross section of the species under consideration. Traditionally this is accomplished by referring all Raman lines to the ones of N_2 or O_2 whose cross section are well-known [1].

Interpretation of vibrational levels of water vapor does not represent a critical issue, however interpretation of the Raman spectra during phase transitions e.g., while homogeneous or heterogeneous freezing occur or in supercooled state, require some further research work. This has been documented in the past by divergences between *ab initio* calculations, numerical approximations and laboratory experiments [2-8] and, of particular importance here, when cloud strata in supercooled state undergoes homogenous or heterogeneous nucleation [9, 10]. In these cases the intramolecular high frequency OH stretch mode shows significant changes around the isosbestic point in the spectral region 3000 to 3800 cm^{-1} as temperature decrease from ambient to -24 ^oC as seen by the polarimetric sensitive Raman spectra [11]. And, as temperature lowers to -35 ^oC and even lower, the asymmetric hydrogen bond (<175 cm^{-1}) [12-15] is observed to decrease bond fluctuation consistent with an increase in the formation of large structures polyhedral clusters in the region < 50 cm^{-1} [16]. (see Figure 1).

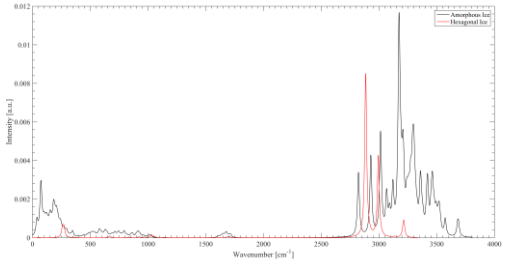

Figure 1. Theoretical Computation of Raman Spectrum of amorphous and hexagonal ice structures based on CASTEP. Lorentzian smearing of 20 cm^{-1} at 200K and 10 cm^{-1}at 290 K respectively.

This complicated physicochemical processes that can be investigated by laser spectroscopy need to be further studied in a Lidar configuration to

provide more sophisticated aerosol-cloud freezing insights into models.

Furthermore, the spectroscopic information provided by this new Raman Lidar will be combined with the determinations of dynamic and microphysics structure of aerosols and clouds layers by means of polarimetric backscatter determination [27, 28]. The polarimetric-Raman capability will allow identifying the thermodynamic processes of water while in presence of aerosols and cloud, identifying non-spherical scatters, and detecting ice formation as well as estimation of crystal shape and their morphological changes as they depends on the depolarization ratio at the laser line. Determination of atmospheric trace gas in the presence of aerosols is fundamental in studying physicochemical processes in multiphase and multicomponent atmospheric chemistry. One of these processes is the aerosol seeding cloud formation or the role of aerosol surfaces assisting heterogeneous ice nucleation or chemical reaction on ice surfaces [17].

Since the inception of Raman Lidar methodology by Cooney [18] the technology had significantly evolved to a level that now it allows simultaneous determination of several atmospheric chemical components using either Raman lidars or combined Differential Absorption Raman based lidars to profile N_2, O_2 and H_2O, SO_2, O_3 and aerosols; see review book edited by Weitkamp [19]. Most typical Raman Lidars [1,20] involve the use of dedicated custom made spectrometric boxes to spectrally resolve several molecular Raman features stimulated by laser radiation as a function of height. This instrumentation currently available operates in the visible and near UV normally stimulated by 532 and 355 nm laser excitation respectively and in the UV-solar blind zone [19]. An example of the latter are tropospheric ozone lidar working at 266 nm with Raman generation in the emission [21] and using 266 nm as laser excitation and Raman backscatter from the atmosphere [22].

On the other hand, Raman lidars operating in the visible region are limited to nighttime dark-sky conditions because background solar radiation levels during daytime surpasses the Raman associated photon counting signal. In most of the cases and depending on the actual latitudinal location the background radiation can top several order of magnitudes the photon count level of the backscattering Raman signal. Some advances including Fabry-Perot etalons in the lidar receiver have overcome partially this issue [23]. Lidars operating in the UV solar blind region, in addition to be eye-safe, enhance the backscattering Raman cross section because of the short laser wavelength typically <300 nm but they verify strong absorption in the ABL due to ozone limiting their operation range [22]. Lidars operating in near UV wavelengths in general optimize the trade-off between maximizing the Raman cross section while maintaining low level of background radiation. Still they require the use of complicated optical arrangements using multiple detectors and multichannel data acquisition receivers. A recent example [24] demonstrated measurement of spectrally resolved water vapor and liquid Raman bands using a dispersive spectrometer coupled to a multichannel detector containing 32 integrated photomultipliers units fiber coupled to the spectrometer exit port.

It is clear that in order to optimize the instrumental range, keeping the Raman cross section high enough and reducing background radiation the laser stimulation has to be in near UV. However at shorter laser excitation wavelengths the Raman spectral separation narrows making the optics significantly more expensive. In this work, therefore we concentrate in demonstrating the feasibility of this Lidar spectroscopy sacrificing signal-to-noise ratio and ranging capability in selecting 532 nm as laser excitation. Nevertheless operating at this wavelength allows a spectral distance between Raman bands to be achieved within reasonable off-the-shelf optics.

2. LIDAR SIMULATION

A simulation of the Raman lidar returns in MCPS (10^6 counts per second) was performed for the main Raman lines to ensure detection limits, maximum vertical resolution and minimum averaging time. The simulation was initialized by radiosonde profile assuming specific atmospheric properties and optical characteristics in the lidar emission and receiver. This simulation allows evaluating the level of signal to be expected in the Raman channels. The lidar equation was implemented including the terms of spectral extinction α [m^{-1}] and backscattering β [sr^{-1} m^{-1}] [25] and the Raman scattering cross sections of

the main atmospheric features N_2, O_2 and H_2O (see Table 1). The following expression shows a compact form of the Raman-Lidar equation as function of the detected wavelength (X).

$$S_X(z) = \frac{E.A}{z^2}.\eta_X.O(z).N_X(z).\sigma_X^{RAM}(\lambda^{RAY},\lambda_X^{RAM}).Tr(z,\lambda^{RAY}).Tr(z,\lambda_X^{RAM})$$

E is the laser energy per pulse, A is the telescope effective collecting area, z is the height, η_X optical throughput at the Raman wavelength (λ_X^{RAM}), $O(z)$ overlapping lidar function, $N_X(z)$ concentration profile of the species of interest, $\sigma_X^{RAM}(\lambda^{RAY},\lambda_X^{RAM})$ Raman cross section of the species of interest depending of the laser stimulation λ^{RAY} and λ_X^{RAM} the Raman wavelength shift, $Tr(z,\lambda^{RAY})$ is the Rayleigh transmission of the atmosphere, including molecules and aerosols, at the laser wavelength and $Tr(z,\lambda_X^{RAM})$ is the atmospheric transmission at the Raman wavelength in the time of flight returning to the telescope.

In this case it was considered a uniform aerosol vertical concentration profile in the ABL and wavelength scaling giving a specific Angstrom coefficient to scale the spectral extinction due to aerosols [26]. The simulation includes a random noise signal level based on a Poisson distribution to simulate real noise photon-detection conditions and the spectral gain curve associated to the detector. The MCPS photon count rate is giving at the entrance of the spectroscopic device. The optical throughput of the device that produces the spectroscopy of the backscattered signal strongly changes depending on the spectral characteristics of the analyzer (e.g., dichroic mirrors and filters). The laser emission and receiver parameters including the detector characteristics are indicated in Table 2.

Figure 2 illustrate the MCPS simulation of the main Raman channels. Additionally theoretical ab initio calculations of Raman spectra based on hexagon microphysical ice structure and amorphous ice consisting of 20 water molecules for sub-freezing temperatures and the theoretical Raman spectrum of an amorphous ice consisting of 20 water molecules is shown in Fig. 1. This information combined to Fig. 3 suggests that strong changes in a band around ~ 3100 cm^{-1} will indicate the formation and presence of ice while liquid should be determined after the isosbestic point where ice features are not prominent ~ 3370 cm^{-1}.

Table 2. 532 nm - Raman Lidar Simulation

Laser Emission Surelite SL II 10 Continuum Lasers	
Wavelength	1064.0 / 532 nm
Linewidth	1.0 cm^{-1}
Pulse repetition frequency	10 Hz
Energy per pulse	650 / 300 mJ
Lidar Receiver	
Smith-Cassegrain	F/5
Primary mirror diameter	50 cm
Focal	2.5 m
Custom Spectrometer	
Dichroic / Razor filters based	F/5 input
Optics and Fiber Optic coupler	Adaptor to F/2.5 coupled to fiber NA=0.2 – 1 mm core
Detection	
Hamamatsu PMT	H10720-20
Peak wavelength	630 nm
Cathode Radiant Sensitivity	78 mA/W
Cathode Quantum Efficiency	0.02
Detector Gain	10^6
Accumulation time	1 min.
Vertical resolution	1.5 m
Angle tuning Raman features	607 nm N_2 - 2331 cm^{-1} 643 ice - 3175.3 cm^{-1} 650 liquid - 3373.6 cm^{-1} 660 nm H_2O - 3651cm^{-1}

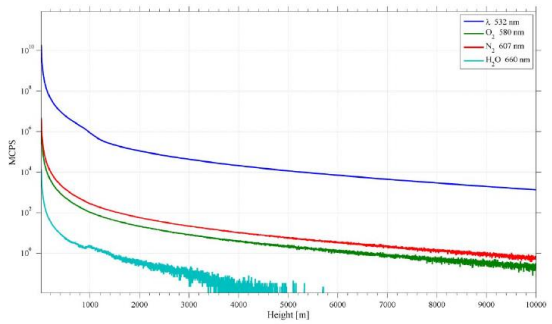

Figure 2. Raman Lidar Simulation. MCPS for 532 nm and Raman lines: O_2 at 580 nm; N_2 at 607 nm and H_2O at 660 nm. Thermodynamic profile from the NWS-PAFA June 21, 2006 at 00UTC (3 PM-AKT). ABL height was at 1km, entrainment zone thickness of 200 m and ozone concentration set to 40 ppb both ABL and free troposphere. Aerosol optical thickness at 380 nm 0.3, scaling wavelength Angstrom coefficient 1.3 and backscatter to extinction ratio of 0.012 sr^{-1}.

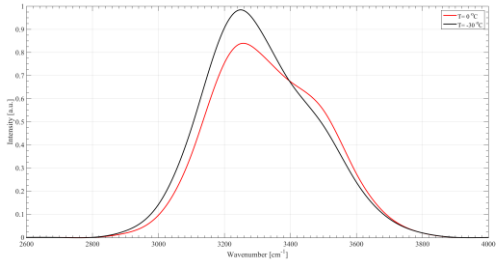

Figure 3. Raman Spectra of Water clusters, adapted from [11].

3. INSTRUMENT DESIGN

The lidar emitter is based on a frequency doubled Nd:YAG pulsed laser operating at 532 nm. The

lidar receiver is based on a Smith-Cassegrain F/5 and 0.5 m primary diameter with optimized optical throughput for visible spectroscopy. In the receiver, after splitting the linear polarization modes (S and P), the telescope is fiber coupled to a spectrometer designed to separate the vibrational Raman lines corresponding to N_2, H_2O and the Raman bands corresponding to Raman bands of ice at 3175.3 cm^{-1} and liquid 3373.6 cm^{-1} content. The instrument layout is shown in Figure 4.

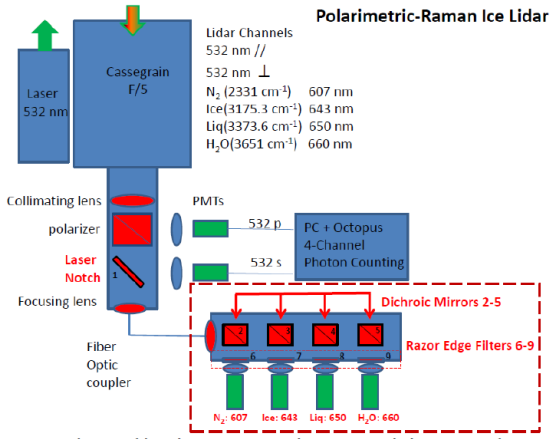

Figure 4. Polarimetric-Raman Ice Lidar Optical Layout.

4. CONCLUSIONS

A new lidar system is being developed to investigate aerosol-cloud processes and composition in the lower troposphere. In this presentation a demonstration of feasibility will be presented illustrating several case example in high latitude polar atmosphere.

ACKNOWLEDGEMENT

To the US-National Science Foundation grant AGS-1443222 and to the EU 2013-program Advanced Spectroscopy in Chemistry, Complutense University of Madrid, Spain.

REFERENCES

[1] Turner D. D. and D. N. Whiteman. 2002. Handbook of Vibrational Spectroscopy. Edited by J. M. Chalmers and P. R. Griffiths. John Wiley and Sons Ltd, Chichester, 2002.
[2] Sceats M., S. A. Rice and J.E. Butler. 1975. *J. Chem. Phys.*, 63, 12, 5390-5400.
[3] Irish D., T. Jary and C. Ratcliffe. 1982. *Applied Spectroscopy*, 36, 2, 137-140.
[4] Ratcliffe C. and D. Irish. 1982. *J. Phys. Chem.* 86, 4897-4905.
[5] Yeh Y., J.H. Bilgram and W. Kanzig. 1982. *J. Chem. Phys*., 77(5), 2317-2321.
[6] Monosmith W. and G. Walrafen. 1984. *Chem. Phys*. 81, 2, 669-674.
[7] Lee Ch., et al. 1993. *Phys. Rev. B*, 47, 9, 4863-4872.
[8] Walrafen G. 2006. *J. Chem. Phys*., 124, 184505; doi: 10.1063/1.2188942
[9] Angel C.A. *Ann. Rev. Phys. Chem*. 1983.34: 593-630
[10] Sokolov A., J. Hurst and D. Quitmann. 1995. *Physical Review B.*, 51, 18, 12865-12868.
[11] D'Arrigo G. et al. 1981. *J. Chem. Phys*. 75: 4264-4270.
[12] Krishnamurthy S., et al. 1983. *J. Chem. Phys*. 79, 12, 5863-5870.
[13] Kanno H., K. Tomikawa and O. Mishima. 1998. *Chem. Phys. Lett.*, 293, 412-416.
[14] Johari G. and O. Andersson. 2007. *Thermochimica Acta*, 461, 14-43.
[15] Suzuki H., et al., 2012. *J. Chem. Phys*., 136, 234508; doi: 10.1063/1.4729476.
[16] Hare D.E. and S.M. Sorensen. 1990. *J. Chem. Phys.*, 93, 1, 25:33.
[17] Hoose C. and O. Möhler. 2012. *Atmos. Chem. Phys.*, 12, 9817–9854.
[18] Cooney J. 1969. *J. Appl. Meteor*. 9, 182-184.
[19] Weitkamp C. 2005. Springer. pp 455.
[20] Di Girolamo P. et al. 2004. *Geophys. Res. Lett.* 31, L01106, doi:10.1029/2003GL018342.
[21] Ancellet G. and F. Ravetta. 1998. *Appl. Opt.*, 37, 24, 5509-5521.
[22] Froidevaux M., et al. 2013. *Advances in Water Resources*. In press.
[23] Arshinov, Y. F., et al. 2003. Proceedings of the *ISTP* 2003, 142-144.
[24] Lui F. and F. Yi. 2013. *Appl. Opt.*, 52, 28, 6884-6895.
[25] Fochesatto, J., et al. 2004. *Advances in Space Research*, *34*, 10, 2227-2231.
[26] Ristori, P., et al. 2003. *Optics and Laser in Engineering*, *40*, 91-104.
[27] Fochesatto, J., et al. 2005. *Proc. of SPIE, 5887*, doi: 10.1117/12.620970.
[28] Fochesatto, J., et al. 2008. *IJHSES. 18, 3, 713-726.*